Journal of Engineering Science and Technology
Vol. 20, No. 6 (2025) 1762 - 1781

NUMERICAL SIMULATION ON PERFORMANCE ENHANCEMENT IN AXIAL FLOW TURBINES USING VENTURI-INTEGRATED BLADE DESIGN

P. N. VASANTH SUDARSHAN*, D. MADHESH

Department of Mechanical Engineering, Academy of Maritime Education and Training Deemed to be University, Kanathur, Chennai, Tamil Nadu 603112, India
*Corresponding Author: vasanthpurushothaman@gmail.com

Abstract

Turbine performance and efficiency are vital for optimizing gas turbine engines, influencing fuel consumption and operational limits. This study introduces an innovative blade design integrating venturi pipes to enhance aerodynamic performance and structural integrity. By embedding venturi pipes within turbine blades, the design accelerates flow, increases exit velocities, and reduces flow separation. Using 3D numerical simulations, two venturi-integrated designs were analysed: one with venturi pipes in the stator blades and another incorporating them in both stator and rotor blades. Results show a 5.39% increase in exit velocity with stator-only modifications and an 8.82% increase when applied to both blade sets. Additionally, the venturi effect energizes the boundary layer, enhances flow acceleration, and reduces aerodynamic losses, leading to improved turbine efficiency. The venturi-integrated design offers significant performance gains without major modifications to the overall blade geometry, making it suitable for both existing and new turbine systems. By combining aerodynamic enhancements with structural benefits, this study demonstrates the potential of venturi integration to revolutionize turbine performance, offering a practical and efficient solution for modern gas turbine applications.

Keywords: Axial flow turbine, Blade design modification, Computational fluid dynamics, Rotor and stator blades, Turbomachinery performance enhancement, Venturi effect.

1. Introduction

Turbines are essential components in modern energy and propulsion systems, designed to convert the energy of a moving fluid-whether gas, steam, or water-into beneficial mechanical work. They play a critical role in a variety of industries, such as aviation, marine, oil and gas, and power generation. In heavy industries, by harnessing the kinetic energy from high-pressure fluids, turbines drive rotating machinery such as compressors and electric generators. Their design involves multiple stages of blades or vanes, which guide the fluid through a controlled expansion process, transforming the fluid's energy into rotational motion. Advances in turbine technology, particularly in enhancing aerodynamic efficiency and thermal performance, continue to push the boundaries of power output and operational efficiency in both stationary and mobile applications [1].

Traditional strategies to improve turbine performance have focused on optimizing blade profiles. Blade profile optimization, including topology-based approaches, has shown significant aerodynamic improvements [2, 3]. However, the resulting complex geometries often pose manufacturing challenges, increasing structural mass and compromising aerodynamic integrity despite the use of advanced fabrication methods like casting and forging. These limitations underscore the need for simpler, more manufacturable innovations such as passive flow control. While these conventional methods have advanced turbine performance, they are increasingly constrained by manufacturing feasibility and structural trade-offs. In light of this, the present study proposes a novel Venturi-integrated blade design to passively accelerate internal flow, enhance exit velocities, and reduce boundary layer separation. This approach aims to deliver aerodynamic improvements without extensive external modifications or manufacturing complications. However, gaps remain in system-level integration and experimental validation, pointing to the need for continued exploration of such innovative design concepts.

Passive and active flow control strategies have been extensively explored to improve turbine efficiency, each presenting unique benefits and limitations. One passive method involves surface-mounted rectangular bars to manage boundary layer transition by promoting early reattachment and reducing separation losses in low-pressure turbine conditions [4]. However, their effectiveness is highly sensitive to Reynolds number and turbulence intensity, and they introduce additional drag and manufacturing complexity for rotating blades. Active techniques, such as synthetic jets, offer dynamic control over surface boundary layers without physical protrusions. These zero-net mass flux actuators can delay separation and modify pressure distributions [5]. Despite their promise, their application in rotating turbomachinery is limited by actuator complexity, energy requirements, and operational reliability concerns in harsh environments.

Innovations in tip design, like winglets and cavity tips, have shown moderate success in reducing leakage losses. While Zhou et al. [6] reported localized benefits with winglet tips, particularly near the leading edge, performance gains diminished downstream, making consistent effectiveness across the blade span difficult to achieve. At the endwall level, features such as leading-edge fillets have been shown to weaken horseshoe vortices and reduce secondary flow losses [7]. Yet, their impact is confined to specific regions and demands high geometric precision, limiting their scalability. Similarly, endwall contouring has demonstrated reduced

secondary kinetic energy and smaller vortices in transonic cascades [8], though improvements in downstream mixed-out losses remain inconsistent due to complex mixing and compression effects at high speeds.

Overall, while these techniques provide measurable aerodynamic benefits, they often face challenges related to localized effectiveness, integration complexity, and manufacturability. In contrast, the current study proposes a Venturi-integrated blade concept that passively accelerates internal flow and energizes the boundary layer, reducing separation without altering the external geometry. This enables performance gains across the blade span while maintaining manufacturing feasibility through additive methods.

The Venturi effect, rooted in the principles of continuity and Bernoulli's equation, describes how fluid velocity increases and pressure decreases in a constricted flow section. This phenomenon, named after Giovanni Battista Venturi, has been widely applied to enhance flow regulation and energy efficiency. Integrating Venturi geometries within turbine blades leverages this effect to accelerate internal flow and boost exit velocities through strategically designed convergent sections [9]. For instance, Tan et al. [10] developed a Variable Area Cavitating Venturi (VACV) for precise oxidizer mass flow control in hybrid rocket motors. Their experiments confirmed highly accurate and stable flow delivery using the Venturi mechanism. While this application differs from turbine blade flows, the underlying principle of controlled flow acceleration remains directly relevant.

Similarly, Beller [11] examined Venturi-shaped casings for wind turbines in urban environments, demonstrating increased local wind velocities and improved energy capture over conventional geometries. Although the context and scale differ, this study further supports the effectiveness of Venturi-based designs in enhancing flow performance within confined aerodynamic systems. Together, these works-from rocket propulsion to urban wind energy-provide foundational evidence that the Venturi effect can be effectively harnessed to improve internal blade aerodynamics and energy efficiency in gas turbines.

In the proposed design, a series of small venturi pipes are embedded within the turbine blade, running from the leading edge towards the trailing edge. These pipes have a larger inlet diameter that gradually decreases along the camber line of blades, creating the necessary constriction for the Venturi effect to occur. As the main flow passes over the blade surface, a portion of it enters these venturi pipes. The flow accelerates as it moves through the converging section, exiting at a higher velocity at the trailing edge of the blade. This high-velocity jet mixes with the main flow, potentially increasing the overall exit velocity of the turbine stage. The key advantages of this approach include increased exit velocity, boundary layer control, structural benefits, and minimal changes to external blade profile.

The primary objective of this study is to investigate the potential performance enhancement of axial flow turbines through the integration of venturi pipes within turbine blades. Specifically, the objectives of the research are to:

- Develop a novel blade design incorporating internal venturi pipes within turbine blades.
- Conduct 3D numerical simulations to evaluate the performance of this new design compared to conventional turbine blades.

- Analyse the effect of venturi integration on turbine exit velocity and overall performance.
- Assess the potential benefits and limitations of this innovative approach.

To achieve these objectives, a comparative study has been conducted on three distinct cases:

- Case 1: Base model with conventional turbine blades and vanes (no venturi pipes).
- Case 2: Modified design with venturi pipes integrated into the Nozzle Guide Vanes (NGVs) only.
- Case 3: Modified design with venturi pipes integrated into both NGVs and rotor blades.

This study introduces a novel turbine design concept by integrating venturi pipes within axial flow turbine blades to enhance performance and structural integrity. By embedding venturi mechanisms in both stator and rotor blades, the design leverages the Venturi effect to increase fluid exit velocity, improving turbine efficiency and power output. Convergent slots in hollow turbine blades also act as stiffeners, enhancing structural strength without altering the external blade profile, ensuring seamless integration with existing frameworks. Using 3D numerical simulations, the study demonstrates significant performance gains, making this innovative approach a promising solution for optimizing turbine efficiency.

2. Method

The design of an efficient axial flow turbine is a complex, multidisciplinary process that involves aerodynamics, thermodynamics, and structural mechanics. This section provides an in-depth look at the turbine design process, with a particular focus on how the venturi-integrated concept was incorporated into the design workflow.

2.1. Turbine design specifications

The preliminary design phase establishes the basic parameters of the turbine based on the desired performance characteristics. For this study, we selected a single-stage axial flow turbine with a low pressure ratio and power output in the order of 1 kW. The turbine specifications are based on the design parameters from Zuniga [12], as outlined in Table 1.

Table 1. Axial flow turbine specification.

Number of Stator Blades	15
Number of Rotor Blades	16
Pressure Ratio	1.2
Angular Velocity	18,000 rpm
Inlet velocity	155m/s
Stagger Angle	30˚
Stator Chord	30 mm
Rotor Chord	28.175 mm
Hub Diameter	60 mm
Shroud Diameter	84 mm

This design includes the thermodynamic analysis of both a custom axial flow turbine and a retrofitted K03 turbocharger. The design methodology was developed for a single-stage axial flow turbine, developed specifically for low-pressure ratio applications (pressure ratio ≈ 1.2), which aligns precisely with the goals of the present study. Thus, the axial turbine modelled in [12] is explicitly a single-stage turbine, making it suitable for foundational performance comparisons in our single-stage modification study involving Venturi integration. Hence, we find this design input to be particularly clear and convenient for the research, as it provides a solid foundation for demonstrating the novelty of the proposed modifications and innovations in turbine performance.

2.2. Detailed aerodynamic design

2.2.1. Blade profile generation

With the basic stage parameters established, we proceeded to the detailed aerodynamic design of the blade rows. For the conventional (non-venturi) blade design, we used a parametric approach to generate the blade profiles. The method, similar to that described by Köller et al. [13], involves defining a mean camber line based on the required flow turning, superimposing a thickness distribution to create the pressure and suction surfaces, and applying leading and trailing edge radii. For the venturi-integrated design, we modified this process to incorporate internal pipes along the camber line: the basic external profile was generated as in the conventional design, internal venturi pipes were created from the leading edge toward the trailing edge, and the venturi duct geometry was carefully shaped to ensure smooth transitions along the blade curvature and minimize losses.

2.2.2. Blade geometry and venturi integration

The 2D blade profiles were stacked to create the 3D blade geometry. We employed a straight stack for simplicity, although more complex stacking techniques (e.g., lean or sweep) could be explored in future optimizations. The design of the venturi pipes was a critical aspect of our novel approach. We based our design on classical venturi pipe principles, as described by Hollingshead et al. [14].

Key considerations included setting the inlet to throat area ratio to almost 3:1 based on preliminary CFD studies, optimizing the convergence angle to minimize entrance losses. The study [15] stated that keeping divergence below 5° helps maintain better outlet velocity uniformity and suppresses reverse flow and separation, especially in confined geometries like turbine blade ducts. Hence, this research maintains the divergence angle below 5° to prevent flow separation in the diffuser section and determining the number and distribution of pipes through an iterative process, balancing performance gain against structural considerations. This provides an optimal balance between diffusion and aerodynamic stability. The baseline turbine blade geometries for both the NGVs and rotor blades were designed based on standard aerodynamic principles for axial flow turbines. Figures 1(a) and (b) illustrate the blade profiles for the NGVs and rotor blades, respectively.

The proposed axial flow turbine consists of first row of Nozzle Guide Vanes (NGV's) with 15 blades and second row rotor with 16 blades. These blade counts are such that the flow domain is rotationally periodic; this allows modelling a portion of geometry for numerical simulation, i.e.) single rotor and single stator

blade geometry. Furthermore, it helps prevent wake–vortex alignment, which can otherwise lead to aerodynamic resonance and unsteady flow phenomena. This deliberate asymmetry promotes better flow mixing, reduced acoustic tones, and improved overall stage efficiency by disrupting the periodic wake shedding and minimizing aerodynamic losses across the blade rows.

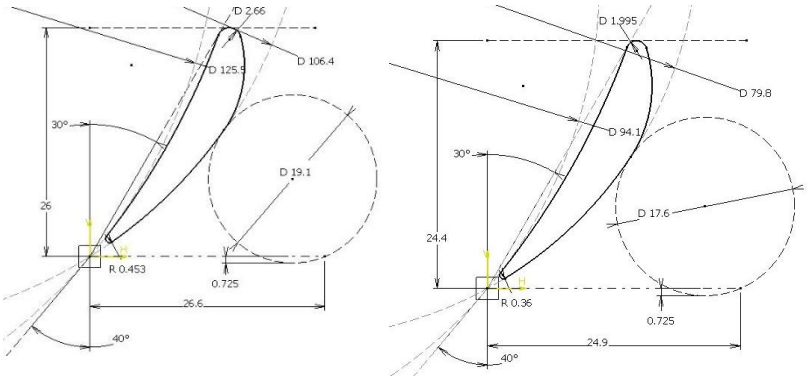

(a) NGV. **(b) Rotor.**

Fig. 1. Blade profile.

For the venturi-integrated designs (Cases 2 and 3), we incorporated a series of convergent pipes within the blade structure. The design parameters for these venturi pipes are as follows:

- Inlet diameter: 1 mm
- Outlet diameter: 0.3 mm
- Number of pipes per blade: 7
- Spacing between pipes: 1.5 mm along the blade height

The ratio of inlet to outlet diameter (3:1) was chosen to optimize the venturi effect while considering manufacturing feasibility and the risk of flow blockage. The number and distribution of Venturi tubes inside the turbine blades were determined through an iterative parametric design process. CFD simulations were run with varying numbers of tubes per blade (ranging from 3 to 10), and it was observed that 7 tubes per blade provided the best balance between flow acceleration and pressure recovery without inducing excessive structural stress. Figure 2 provides a cross-sectional side-view of a turbine blade with integrated venturi pipes.

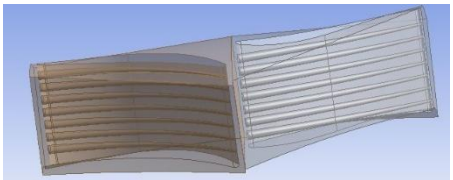

Fig. 2. Transparent flow volume with clear view of convergent pipes.

To visualize the integration of venturi pipes within the turbine blades, a transparent flow volume model was generated. This model clearly shows the placement and

orientation of the convergent pipes within the blade structure, providing a comprehensive view of the design enhancements. The transparent volume helps in understanding how the pipes are positioned relative to the overall blade geometry.

To analysed section-wise performance, the exit velocity was measured at three spanwise locations along the rotor blade trailing edge plane:

- Hub: 10% span from the inner diameter
- Midspan: 50% span (blade centreline)
- Tip: 90% span near the shroud

At each of these locations, area-averaged velocity magnitudes were extracted on a cross-sectional surface normal to the flow direction, just downstream of the rotor trailing edge.

The 2D assembly diagrams in Figs. 3(a), (b) and (c) illustrate the localized, axisymmetric configurations of the turbine blade designs for Case 1, Case 2, and Case 3, respectively. These visualizations clearly distinguish the distribution of Venturi ducts in the stator and rotor blades across each configuration.

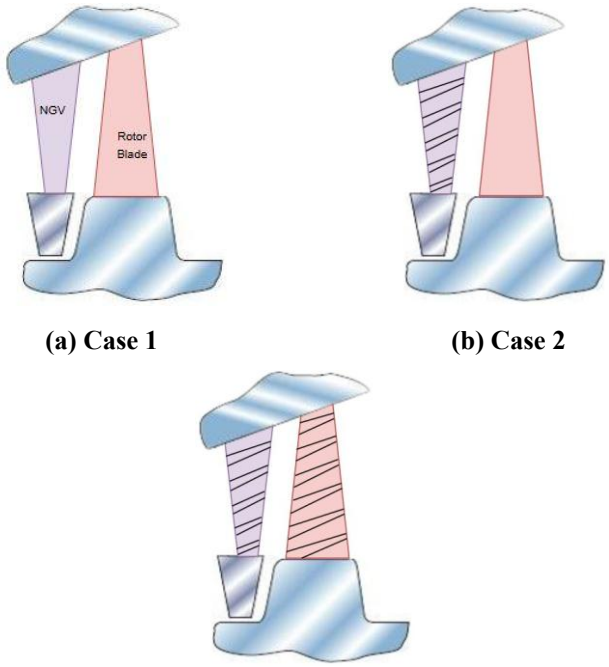

(a) Case 1 **(b) Case 2**

(c) Case 3

Fig. 3. Assembly diagram.

2.3. Numerical simulation setup

The 3D numerical simulations were performed using ANSYS Fluent within the ANSYS Workbench platform. A pressure-based coupled solver was adopted, suitable for steady-state compressible flow analysis in turbomachinery. The turbulence was modelled using the k–ω Shear Stress Transport (SST) model,

maintaining a y^+ value between 1-5 with enhanced wall treatment. Mesh quality was ensured by maintaining a maximum skewness below 0.8 and an aspect ratio under 10. Mesh independence was verified through a grid convergence study to validate the accuracy and stability of the simulation results.

At the inlet, a velocity boundary condition of 155 m/s was applied, while a static pressure boundary condition was imposed at the outlet. Blade surfaces were modelled as no-slip walls, and periodic boundary conditions were applied along the side faces. The stator-rotor interface was treated using a frozen rotor approach, assuming a steady-state relative frame of reference.

Geometry and mesh generation

Three-dimensional models of the turbine stage were created using CAD software. To reduce computational resources, only a single NGV and a single rotor blade were modelled, utilizing rotational periodicity. Mesh matching across periodic faces was ensured, maintaining element count variation below 1%.

Unstructured tetrahedral meshes were generated for each model using ANSYS Workbench (Fig. 4). To perform rotationally periodic, it is necessary that the number of elements should be same on both the faces, so while meshing match control between two side faces are adopted to get same surface mesh on both the sides. The accuracy of any CFD solution greatly depends on the quality mesh used. So, mesh quality check was performed.

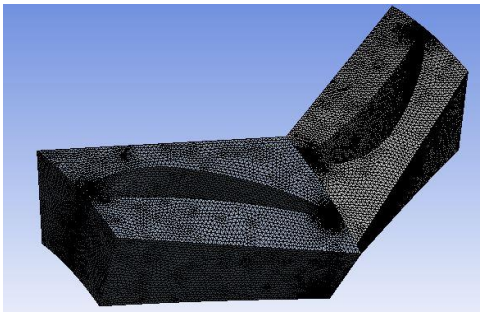

Fig. 4. Meshed flow volume of base model.

Figure 5 presents a grid independence study, which is a crucial step in CFD simulations to ensure that the numerical results are not significantly affected by the size or number of mesh elements used in the simulation. The graph likely plots the number of grid elements (or element size) on the x-axis and a key output parameter, such as outlet velocity, pressure drop, or efficiency, on the y-axis. Initially, as the mesh is refined (increasing number of elements), the results change significantly. This study was conducted by evaluating outlet velocity across mesh sizes ranging from 50,000 to 500,000 elements. As shown in Fig. 5, the outlet velocity stabilized at approximately 204 m/s beyond 350,000 elements, with less than 0.5% variation. Thus, the final simulations used a mesh with ~350,000 elements, ensuring accuracy while optimizing computational cost, with a maximum skewness below 0.8 and aspect ratio maintained under 10. This validates the accuracy of the numerical model used in the study. Convergence was ensured by achieving residual thresholds of 1×10^{-5} for continuity, momentum, energy, and turbulence equations.

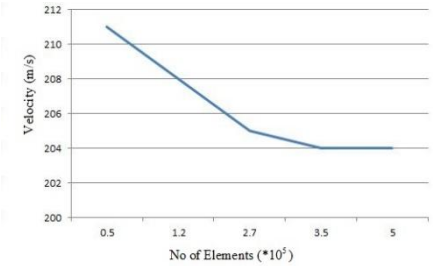

Fig. 5. Grid independence study.

2.4. Flow visualization

Advanced flow visualization techniques were employed to better understand the complex flow patterns introduced by the venturi pipes. The acceleration of fluid flow is achieved using venture pipe or a converged duct. So, to increase the exit velocity of the turbine, set of convergent pipes are placed inside the blade along the camber. To obtain best venture effect, the ratio of inlet to outlet diameter of the convergent duct is kept as 3:1. The inlet diameter of the convergent duct is 1 mm, and the outlet diameter is 0.3 mm. totally 7 pipes are placed at a spacing 1.5 mm along the blade height. Figures 6(a), (b), and (c) show flow volume extraction for Cases 1, 2, and 3.

In Case 1 (conventional design), the flow follows a relatively uniform path through the blade passage. In contrast, Cases 2 and 3 show distinct perturbations in the flow patterns near the exits of the venturi pipes. These perturbations indicate regions of high-velocity flow injected into the main passage, contributing to overall flow acceleration.

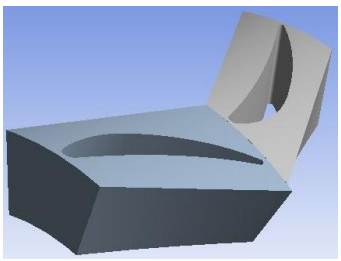

(a) Case 1.

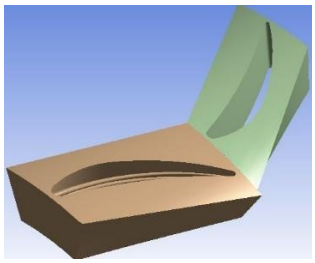

(b) Case 2.

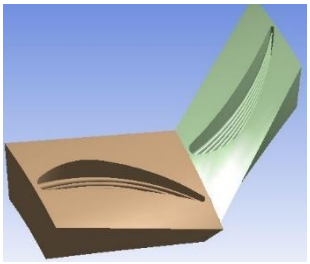

(c) Case 3.

Fig. 6. Flow volume.

3. Results and Discussion

The numerical simulations provided a wealth of data on the flow characteristics and performance metrics for each of the three cases studied. This section presents the key findings, focusing on the impact of venturi integration on turbine performance.

3.1. Outlet velocity comparison

One of the primary objectives of this study was to investigate the effect of venturi integration on the turbine outlet velocity. Tables 2 and 3 summarizes the average outlet velocities for each case and the percentage improvement compared to the base model (simulation, theoretical, and experimental).

The theoretical outlet velocity was obtained using the isentropic flow equations based on the conservation of energy. Assuming steady-state, adiabatic flow through the turbine stage, the following formulation was applied:

$$v_{out} = \sqrt{v_{in}^2 + 2(h_{in} - h_{out})} \quad (1)$$

where, v_{in} is the inlet velocity, h_{in} and h_{out} are the enthalpies at the inlet and outlet of the turbine, respectively.

Upon solving Eq. (1), the theoretical outlet velocity of 198 m/s was achieved, which is in close agreement with the CFD simulation result of 204 m/s, with a percentage error of 3%.

Table 2. Comparison of CFD result &theoretical.

	CFD Simulation	Theoretical	Experimental (as achieved by Zuniga [12])	% Error (Compared to Theoretical Output)
Outlet Velocity (m/s)	204	198	204	3

Table 3. Result comparison of three models.

	Inlet (m/s)	Outlet Velocity (m/s)	% Improvement
Case 1	155	204	
Case 2	155	215	5.39%
Case 3	155	222	8.82%

These results demonstrate a clear improvement in outlet velocity with the integration of venturi pipes. Case 2, with venturi pipes in the NGVs only, shows a 5.39% increase in outlet velocity compared to the base model. Case 3, with venturi pipes in both NGVs and rotor blades, exhibits an even more significant improvement of 8.82%. Additionally, it is proved that the achieved CFD output and the experimental results of the base model achieved by Burdett and Povey [16] align well. Further, the venturi integration successfully enhances flow acceleration, resulting in higher exit velocities compared to the base model. In an ideal, perfectly controlled system, identical inflow and boundary conditions should result in the

same outflow conditions. However, in practical CFD simulations and experimental setups, minor variations in numerical approximations, turbulence modelling, and mesh resolution introduce deviations in flow parameters at the outlet.

3.2. Velocity contours

To understand the flow behaviour within the turbine stage, we analysed velocity contours at various cross-sections. Figures 7(a), (b) and (c) show the velocity contours at the mid-span of the turbine stage for Cases 1, 2, and 3, respectively.

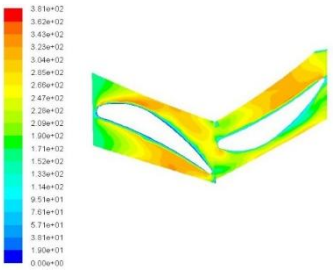

(a) Case 1.

Note: NGV is on the left and rotor is on the right. Colour bar represents velocity magnitude in m/s. Flow moves from left to right.

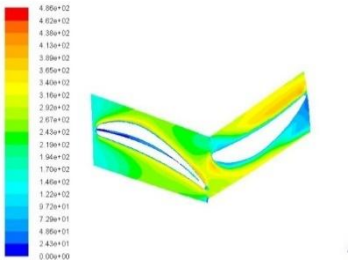

(b) Case 2.

Note: This output shows accelerated flow downstream of the venturi ducts in the stator section.

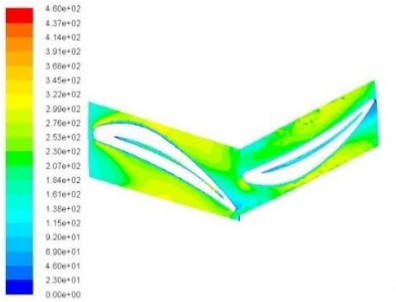

(c) Case 3.

Note: This indicates enhanced flow acceleration through both blade rows.

Fig. 7. Velocity contour.

3.3. Pressure distribution

The pressure distribution within the turbine stage provides insight into the energy conversion process and the impact of the venturi pipes. Figures 8(a), (b) and (c) present the static pressure contours for Cases 1, 2, and 3, respectively.

Key observations from the pressure contours include:

- All cases show the expected pressure gradient from the NGV inlet to the rotor outlet, driving the flow through the turbine stage.
- In Cases 2 and 3, we observe localized low-pressure regions at the exits of the venturi pipes, corresponding to the high-velocity jets observed in the velocity contours.
- Case 3 exhibits the most pronounced pressure variations, particularly in the rotor blade passage, indicating a more complex flow structure and potentially higher energy extraction.

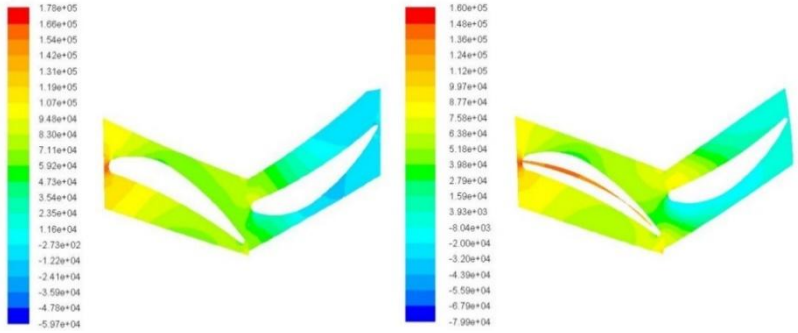

(a) Case 1. **(b) Case 2.**

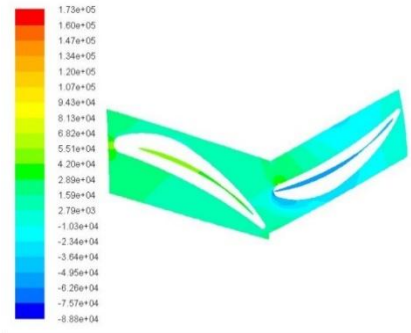

(c) Case 3.

Fig. 8. Static pressure contour.

3.4. Flow streamlines

To visualize the flow path through the turbine stage and the effect of the venturi pipes, we generated 3D streamlines for each case. Figure 9(a), (b) and (c) show these streamlines, coloured by velocity magnitude.

These streamlines provide valuable insights into the flow behaviour:

- 1. In Case 1, the streamlines follow smooth paths through the NGVs and rotor blades, with gradual acceleration as expected in a conventional turbine design.
- In Case 2 shows distinct high-velocity streamlines emanating from the venturi duct exits in the NGVs. These accelerated flow paths interact with the main flow in the rotor passage, contributing to overall flow acceleration.
- In Case 3, we observe high-velocity streamlines from both the NGV and rotor blade venturi pipes. The interaction of these accelerated flows creates a more complex but higher-energy flow field throughout the turbine stage.

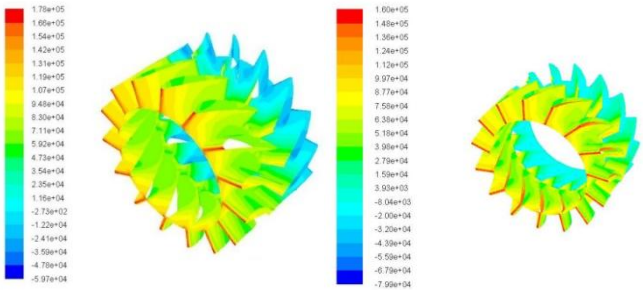

(a) Case 1. **(b) Case 2.**

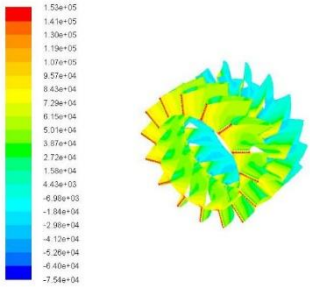

(c) Case 3.

Fig. 9. 3D streamlines.

3.5. Quantitative performance metrics

To quantify the performance improvements, we analysed several key metrics across different blade sections.

3.5.1. Section-wise exit velocity

Table 4 presents the mass-averaged exit velocities at hub, midspan, and tip sections for all three cases.

Table 4. Mass-averaged exit velocities (m/s) at different blade sections.

Section	Case 1	Case 2	Case 3
Hub	198	210	216
Midspan	204	215	222
Tip	192	204	210

Table 4 highlights the impact of venturi-integrated designs on mass-averaged exit velocities at the hub, midspan, and tip across three cases. Case 1 serves as the baseline, while Cases 2 and 3 demonstrate consistent increases in exit velocities, with Case 3 showing the highest values. The values in Table 4 align with the velocity distributions shown in Figs. 7(a), (b) and (c). In Case 1 (as shown in Fig. 7(a)), the velocity profile remains relatively uniform with modest acceleration at the midspan. In Case 2 (Fig. 7(b)), significant flow acceleration is observed downstream of the NGV, particularly at midspan and tip, which corresponds to the increased velocities recorded in Table 4. In Case 3 (Fig. 7(c)), the combined Venturi effect in both NGV and rotor blades results in visibly enhanced velocity fields along the entire span, which directly correlates with the highest values at all three sections in Table 4. This confirms that the local acceleration visualized in the contours is quantitatively captured in the section-wise velocity measurements. These enhancements confirm the effectiveness of venturi integration in improving aerodynamic performance and optimizing airflow, resulting in better overall turbine efficiency.

3.5.2. Loss coefficient analysis

We calculated the total pressure loss coefficient (ω) for each case using Eq. (2) [16]:

$$\omega = (P01 - P02) / (P01 - p1) \quad (2)$$

where P01 is the inlet total pressure, P02 is the exit total pressure, p1 is the inlet static pressure.

Figure 10 compares the spanwise total pressure loss coefficients for three turbine designs: Case 1 (Base Model), Case 2 (Stator Duct), and Case 3 (Stator & Rotor Duct). Case 1 exhibits the highest pressure losses, particularly near the blade tip. Case 2 shows reduced losses, especially in the midspan region, while Case 3 achieves the lowest pressure losses across the span, effectively minimizing tip leakage losses and enhancing airflow control. The analysis confirms that venturi integration, particularly in Case 3, significantly reduces aerodynamic losses, improves flow acceleration, and enhances turbine efficiency. A 3:1 area ratio in venturi ducts offers optimal performance.

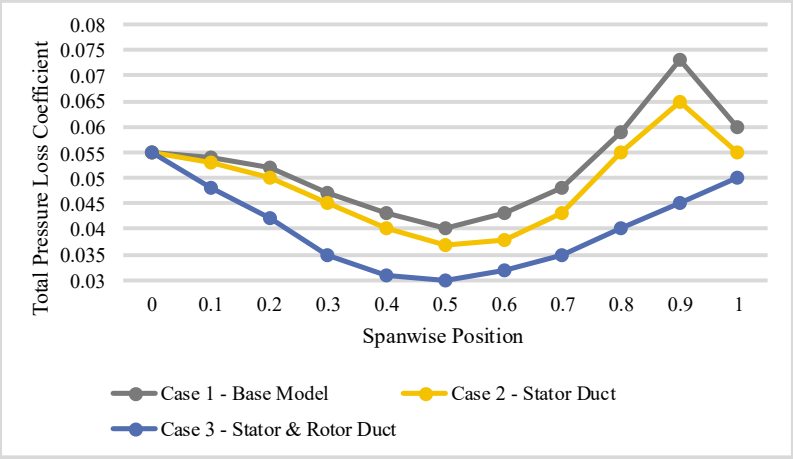

Fig. 10. Spanwise distribution of total pressure loss coefficient.

3.5.3. Efficiency analysis

To validate the performance of the proposed venturi-integrated turbine blade designs, the isentropic efficiency is calculated for three different cases: Case 1 (base model), Case 2 (venturi pipes in the stator blades), and Case 3 (venturi pipes in both stator and rotor blades). Isentropic efficiency is a critical measure of the aerodynamic performance of a turbine. It compares the actual turbine work output to the ideal work output in an isentropic process (i.e., one without energy losses due to friction, heat transfer, etc.). The efficiency can be defined as [17]:

$$\eta = \frac{h_{01} - h_{02}}{h_{01} - h_{0s}} \tag{3}$$

where, h_{01} represents total enthalpy at the turbine inlet, h_{02} represents total actual enthalpy at the turbine outlet, h_{0s} represents total isentropic enthalpy at the turbine outlet.

As per the base model specifications from [18], the axial turbine's final configuration was established with a rotor speed of 78,500 rpm, an outlet pressure of 134 kPa, and an inlet temperature of 900 K, along with an inlet pressure of 200 kPa. Then the efficiency is determined as follows.

$$\eta_{case1} = 81.74\%$$

Similarly, in Table 5, with the introduction of venturi pipes, the efficiencies of case 2 and 3 are determined as 86.45% and 89.02%, respectively. Case 2 and 3 indicate improvements of 4.71% and 7.28%, respectively, compared to case 1. The improvements in efficiency of Cases 2 and 3 over the baseline Case 1 are visualized in Fig. 11. The simulation results highlight key aerodynamic improvements in venturi-integrated designs (Cases 2 and 3). Velocity contours show accelerated flow near blade trailing edges, increasing outlet velocities.

Spanwise pressure analysis reveals a 12% reduction in pressure losses in Case 3 compared to the baseline. Case 3 also achieves higher isentropic efficiency (89.02%) than Case 1 (81.74%), driven by reduced boundary layer losses and enhanced flow acceleration through venturi passages. A two-stage axial turbine developed for Organic Rankine cycle (ORC) applications achieved an overall isentropic efficiency of 83.94%, compared to 78.30% for a single-stage turbine, reflecting a 7.2% improvement [19]. Although the working fluids and operating conditions differ, the aerodynamic principles of flow acceleration and loss minimization are comparable. This supports the fact that our achieved baseline efficiency of 81.74% and improved efficiency of 89.02% fell within a realistic output range of 75% to 90% typically seen in optimized small-scale turbine systems, thereby validating the plausibility of our results.

Table 5. Comparison of isentropic efficiency for different cases.

Case	Isentropic Efficiency	Improvement compared to Case 1
Case 1	$\eta_{case1} = 81.74\%$	-
Case 2	$\eta_{case2} = 86.45\%$	4.71%
Case 3	$\eta_{case3} = 89.02\%$	7.28%

While the outlet velocity improvements as presented in Table 3 (5.39% for Case 2 and 8.82% for Case 3) primarily indicate flow acceleration due to the venturi effect, the efficiency improvement (4.71% for Case 2 and 7.28% for Case 3) reflects a

broader impact that includes both increased kinetic energy at the outlet and reduced aerodynamic losses (such as lower total pressure loss coefficients across the blade passages). The venturi pipes not only increase outlet speed but also improve boundary layer control, minimize flow separation, and reduce energy dissipation across the turbine stage. These secondary aerodynamic benefits contribute to a higher isentropic efficiency gain relative to the direct speed increase alone.

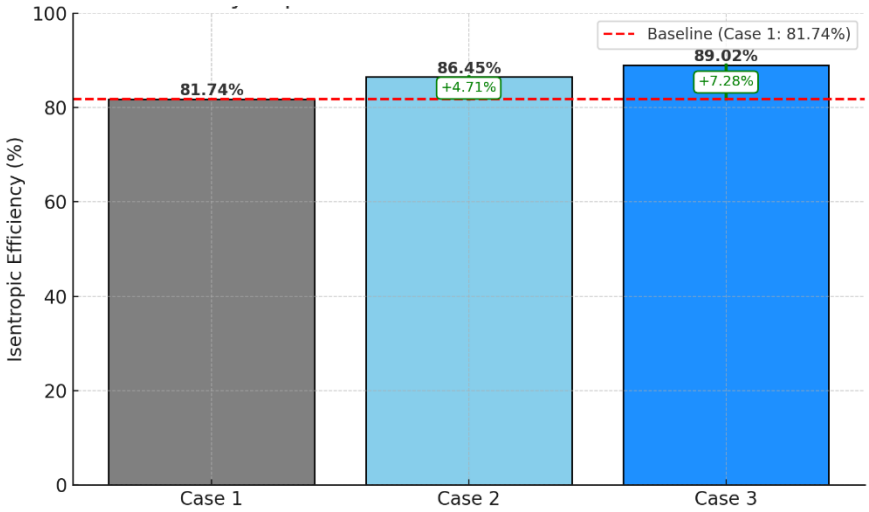

Fig. 11. Efficiency improvement over baseline.

3.6. Coupling of loss reduction, velocity improvement, and efficiency

The improvements observed in exit velocity (Section 3.5.1) and loss coefficient (Section 3.5.2) are physically and thermodynamically coupled and directly influence the overall isentropic efficiency of the gas turbine.

A lower value of ω in Case 3 (as seen in Fig. 10) indicates better pressure recovery and reduced aerodynamic losses, especially near blade tips where leakage and separation are critical. This is a result of the Venturi-induced flow acceleration that re-energizes boundary layers and suppresses recirculation zones.

According to Bernoulli's principle:

$$P + \frac{1}{2}\rho V^2 = constant \tag{4}$$

This shows that an increase in local flow velocity V-as enabled by the Venturi ducts-leads to a corresponding decrease in static pressure but enhances momentum and outlet kinetic energy. These effects translate into higher mass-averaged exit velocities (Table 4) and more uniform velocity distributions at the turbine exit plane, which are crucial for minimizing entropy generation and enabling higher stage work extraction.

This improved flow quality contributes to a reduction in the difference between actual and isentropic enthalpy drops, as captured by the isentropic efficiency. The observed increase in exit velocity and reduction in total pressure loss (lower ω) in Case 3 result in a smaller difference between h_{02} and h_{0s}, thus enhancing

isentropic efficiency. The result is a clear aerodynamic benefit where loss reduction and velocity enhancement act synergistically to improve turbine performance.

3.7. Comparison with existing methods

The proposed Venturi-integrated design introduces internal flow acceleration without altering external blade geometry, distinguishing it from other established turbine performance enhancement strategies. For instance, the study [20] demonstrated that variable fillet configurations near blade-endwall junctions could significantly reduce secondary flow losses by mitigating horseshoe vortex development and delaying boundary layer growth. While this approach improves loss coefficients and near-wall flow stability, it primarily addresses flow separation at the junction, rather than global flow acceleration through the blade core as achieved by the Venturi mechanism.

Sunil et al. [21] investigated contoured endwalls to reduce thermal loads and enhance secondary flow control. Their axisymmetric design achieved notable improvements in film cooling and turbine durability, especially in high-Reynolds-number conditions. Though highly effective for thermal management and endwall loss mitigation, the technique requires precise endwall shaping and is sensitive to coolant blowing ratios, making it more complex to implement across various turbine scales compared to the geometrically internal and scalable nature of Venturi integration.

Zeng et al. [22] focused on squealer tip optimization to minimize tip leakage and enhance aerodynamic sealing through vortex management. Their design tailored squealer dimensions to form effective aero-labyrinth seals, reducing leakage loss particularly under transonic conditions. This technique is advantageous for tip-region flow control, but unlike the Venturi approach, it lacks whole-span flow energization and internal acceleration benefits.

Overall, while variable fillets, contoured endwalls, and squealer tips each target specific loss mechanisms with localized aerodynamic improvements, the Venturi-integrated blade design uniquely provides distributed internal flow enhancement, boundary layer re-energization, and improved exit velocities across the full blade span. Its compatibility with additive manufacturing and minimal impact on external profiles makes it a versatile and scalable alternative for next-generation turbine applications.

4. Practical Feasibility

The integration of Venturi tubes within turbine blades is practically feasible due to recent advancements in manufacturing technologies such as Direct Metal Laser Sintering (DMLS) and Electron Beam Melting (EBM). These additive manufacturing techniques facilitate the precise and accurate formation of intricate internal geometries required by Venturi-integrated designs. However, specific manufacturing limitations should be considered, including challenges related to achieving consistent dimensional precision, potential issues with surface finish quality within internal channels, and residual stresses resulting from rapid heating and cooling cycles inherent to additive manufacturing processes. Despite these constraints, such technologies have been successfully utilized in producing internally cooled turbine blades for high-temperature gas turbine applications, providing a strong precedent for complex internal channel fabrication.

Furthermore, structural integrity concerns associated with integrating Venturi tubes are proactively mitigated by adhering to established design methodologies commonly used in hollow blade structures. Specifically, the Venturi tubes are strategically positioned to enhance aerodynamic performance without compromising mechanical stability. Instead of acting as points of structural weakness, these internal tubes contribute positively by functioning as internal stiffeners, thus bolstering the overall structural robustness of the blades.

Consequently, the slight increase in manufacturing complexity, balanced against operational limitations such as thermal stresses and cyclic loading conditions, remains justified by substantial aerodynamic benefits, including enhanced exit velocity, reduced pressure losses, and improved overall turbine efficiency, underscoring the practical viability of the proposed Venturi integration approach.

5. Conclusion

In this study, a novel axial flow turbine blade design was proposed by integrating Venturi pipes into the stator and rotor components, and its aerodynamic performance was evaluated using 3D numerical simulations. The modified designs demonstrated measurable improvements over the conventional model. Specifically, Case 2, which featured Venturi integration in the stator blades only, resulted in a 5.39% increase in exit velocity and reached an isentropic efficiency of 86.45%, reflecting a 4.71% improvement over the base case. In Case 3, where Venturi pipes were embedded in both stator and rotor blades, the design achieved an 8.82% rise in exit velocity and a corresponding 7.28% enhancement in isentropic efficiency, reaching 89.02%. These results confirm that Venturi integration effectively accelerates flow, reduces pressure losses, and enhances overall turbine efficiency.

Although the improvements are promising, it is important to acknowledge that the simulations were conducted under idealized steady-state and adiabatic assumptions without considering mechanical losses, manufacturing tolerances, or long-term operational degradation. Therefore, while the achieved efficiencies fall within a realistic industrial range of 75–90% reported for optimized small-scale turbines, experimental validation and prototype testing are necessary to fully confirm the practical applicability of the proposed design.

Future work should focus on specific areas such as experimental prototyping of Venturi-integrated blades, investigation of structural integrity under thermal and centrifugal loading, evaluation of manufacturing feasibility using additive manufacturing techniques, and transient simulations to assess the design's robustness under real-world operating conditions. Furthermore, optimization of Venturi geometry for different blade spans and working fluids could be explored to generalize the concept across broader turbine applications. For new turbine designs, the Venturi-integrated concept offers a scalable solution for enhancing stage efficiency without sacrificing structural robustness. Scalability across varying turbine sizes and operating conditions will depend on fine-tuning the Venturi geometry and its distribution across the blade span.

Future work should prioritize experimental validation, prototype development using additive manufacturing, thermal and structural fatigue testing, and transient simulations under fluctuating load conditions. Additionally, optimization studies involving different working fluids and multistage configurations could unlock broader applications across aviation, energy, and marine sectors. In conclusion, the Venturi-integrated blade design

represents a promising, manufacturable innovation with significant potential for enhancing turbine efficiency across diverse real-world contexts.

Nomenclatures

h_{in}	Inlet velocity
h_{out}	Outlet velocity
P01	Inlet total pressure
P02	Exit total pressure
p1	Inlet static pressure
v_{in}	Inlet velocity
v_{out}	Outlet velocity

Greek Symbol

ω	Total pressure loss coefficient

Abbreviations

3D	Three Dimensional
CFD	Computational Fluid Dynamics
DMLS	Direct Metal Laser Sintering
EBM	Electron Beam Melting
NGV	Nozzle Guide Vanes
SSD	Shear Stress Transport

References

1. Hansen, M.O.L. (2015). *Aerodynamics of wind turbines*. Routledge.
2. Sudarshan, P.N.V.; and Devasenan, M. (2025). A comprehensive study of recent studies on the efficiency of axial flow turbines with an investigation on blade profile modifications in stator and rotor assemblies. *Wind Engineering*, 49(2), 557-585.
3. Vatanabe, S.L.; Lippi, T.N.; de Lima, C.R.; Paulino, G.H.; and Silva, E.C.N. (2016). Topology optimization with manufacturing constraints: A unified projection-based approach. *Advances in Engineering Software*, 100, 97-112.
4. Volino, R.J. (2003). Passive flow control on low-pressure turbine airfoils. *Journal of Turbomachinery*, 125(4), 754-764.
5. Glezer, A.; and Amitay, M. (2002). Synthetic jets. *Annual review of fluid mechanics*, 34(1), 503-529.
6. Zhou, C.; Hodson, H.; Tibbott, I.; and Stokes, M. (2017). Effects of winglet geometry on the aerodynamic performance of tip leakage flow in a turbine cascade. *Journal of Turbomachinery*, 135(5), 051009.
7. Zess, G.A.; and Thole, K.A. (2002). Computational design and experimental evaluation of using a leading edge fillet on a gas turbine vane. *Journal of Turbomachinery*, 124(2), 167-175.
8. Taremi, F.; Sjolander, S.A.; and Praisner, T.J. (2013). Application of endwall contouring to transonic turbine cascades: Experimental measurements at design conditions. *Journal of Turbomachinery*, 135(1), 011031.

9. Çengel, Y.A.; and Cimbala, J.M. (2013). *Fluid mechanics*: *Fundamentals and applications*. McGraw-Hill.
10. Tan, G.; Tian, H.; Gu, X.; Meng, X.; Wei, T.; Zhang, Y.; and Cai, G. (2023). Flow feedback control based on variable area cavitating venturi and its application in hybrid rocket motors. *Acta Astronautica*, 211, 238-248.
11. Beller, C. (2008). Layout design for a venturi to encase a wind turbine integrated in a high rise. *Proceedings of the* 2008 *European Wind Energy Conference and Exhibition*, Brussels, Belgium.
12. Zuniga, Y.S.P. (2011). *Design of an axial turbine and thermodynamic analysis and testing of K*03 *turbocharger*. Bachelor's thesis, Department of Mechanical Engineering, Massachusetts Institute of technology.
13. Köller, U.; Mönig, R.; Küsters, B.; and Schreiber, H.-A. (2000). 1999 Turbomachinery committee best paper award: Development of advanced compressor airfoils for heavy-duty gas turbines-Part I: Design and optimization. *Journal of turbomachinery*, 122(3), 397-405.
14. Hollingshead, C.L.; Johnson, M.C.; Barfuss, S.L.; and Spall, R.E. (2011). Discharge coefficient performance of Venturi, standard concentric orifice plate, V-cone and wedge flow meters at low Reynolds numbers. *Journal of Petroleum Science and Engineering*, 78(3-4), 559-566.
15. Li, Z.; Moradi, I.; Nguyen, Q.; Karimipour, A.; Afrand, M.; Tlili, I.; and Incecik, A. (2020). Three-dimensional simulation of wind tunnel diffuser to study the effects of different divergence angles on speed uniform distribution, pressure in outlet, and eddy flows formation in the corners. *Physics of Fluids*, 32(5), 052006.
16. Burdett, D.; and Povey, T. (2022). Analysis of averaging methods for nonuniform total pressure fields. *Journal of Turbomachinery*, 144(5), 051011.
17. Thakare, H.R.; Monde, A.; and Parekh, A.D. (2015). Experimental, computational and optimization studies of temperature separation and flow physics of vortex tube: A review. *Renewable and Sustainable Energy Reviews*, 52, 1043-1071.
18. Panayides, C.; Pesyridis, A.; and Saravi, S.S. (2019). Design of a sequential axial turbocharger for automotive application. *Energies*, 12(23), 4433.
19. Al Jubori, A.M.; Al-Dadah, R.; and Mahmoud, S. (2017). An innovative small-scale two-stage axial turbine for low-temperature organic Rankine cycle. *Energy Conversion and Management*, 144, 18-33.
20. Ananthakrishnan, K.; and Govardhan, M. (2018). Influence of fillet shapes on secondary flow field in a transonic axial flow turbine stage. *Aerospace Science and Technology*, 82-83, 425-437.
21. Sunil, S.; Sunny, T.P.; and Biju, N. (2023). Accomplishments of endwall contouring on heat transfer in a passage of a turbine blade. *Makara Journal of Technology*, 27(2), 68-74.
22. Zeng, F.; Zhang, W.; Wang, Y.; Cao, X.; and Zou, Z. (2021). Effects of squealer geometry of turbine blade tip on the tip-leakage flow and loss. *Journal of Thermal Science*, 30(4), 1376-1387.